Microsc. Microanal. 19, 406–414, 2013
doi:10.1017/S1431927612014341

Microscopy AND Microanalysis

Architecture of the Subendothelial Elastic Fibers of Small Blood Vessels and Variations in Vascular Type and Size

Akira Shinaoka,[1] Ryusuke Momota,[1] Eri Shiratsuchi,[2] Mitsuko Kosaka,[1] Kanae Kumagishi,[1] Ryuichi Nakahara,[3] Ichiro Naito,[1] and Aiji Ohtsuka[1,*]

[1]*Department of Human Morphology, Okayama University Graduate School of Medicine, Dentistry and Pharmaceutical Sciences, 2-5-1, Shikata-cho, Kita-ku, Okayama 700-8558, Japan*
[2]*Research and Development Division, Hayashikane Sangyo Co., Ltd., Shimonoseki 750-8608, Japan*
[3]*Department of Orthopaedic Surgery, Okayama University Graduate School of Medicine, Dentistry and Pharmaceutical Sciences, 2-5-1, Shikata-cho, Kita-ku, Okayama 700-8558, Japan*

Abstract: Most blood vessels contain elastin that provides the vessels with the resilience and flexibility necessary to control hemodynamics. Pathophysiological hemodynamic changes affect the remodeling of elastic components, but little is known about their structural properties. The present study was designed to elucidate, in detail, the three-dimensional (3D) architecture of delicate elastic fibers in small vessels, and to reveal their architectural pattern in a rat model. The fine vascular elastic components were observed by a newly developed scanning electron microscopy technique using a formic acid digestion with vascular casts. This method successfully visualized the 3D architecture of elastic fibers in small blood vessels, even arterioles and venules. The subendothelial elastic fibers in such small vessels assemble into a sheet of meshwork running longitudinally, while larger vessels have a higher density of mesh and thicker mesh fibers. The quantitative analysis revealed that arterioles had a wider range of mesh density than venules; the ratio of density to vessel size was higher than that in venules. The new method was useful for evaluating the subendothelial elastic fibers of small vessels and for demonstrating differences in the architecture of different types of vessels.

Key words: vascular corrosion casting, elastic fiber, elastin, SEM, formic acid digestion, rat, three-dimensional architecture

Introduction

Elastic fibers are multimolecular complexes that contain a cross-linked elastin core surrounded by a mantle of fibrillin-rich microfibrils and several other associated molecules such as fibulin-5 (Kielty et al., 2002). Elastic fibers form when microfibrils link up with elastin-producing-cells via intercalation by fibulin-5. They provide a scaffold for self-assembly of tropoelastin, the precursor of elastin (Hirai et al., 2007). The tropoelastin amino acid sequence has two major domains types: hydrophilic and hydrophobic. The hydrophobic domains are rich in nonpolar residues such as glycine, valine, and proline. The hydrophilic regions are characterized by their high lysine and alanine contents as well as by their involvement in intermolecular cross-linking, which generates elasticity and stability against heat, strong alkali, and strong acids (Wise & Weiss, 2009).

Elastic tissues in the vascular walls are found in three layers: tunica intima, tunica media, and tunica adventitia. These elastic components are observed as complexes of elastic fibers, and their directions depend on the long axis of elastin producing cells; the elastic fibers produced by endothelial cells (ECs) are arranged parallel to the blood flow (internal elastic lamina) while those produced by smooth muscle cells (SMCs) are perpendicular to the blood flow (elastic lamellae) (Farand et al., 2007). The number of elastic lamellae in the tunica media gradually decreases as vessels come to the periphery. Therefore, muscular arteries have fewer elastic lamellae in the tunica media than elastic arteries (Ushiki & Murakumo, 1991). In small vessels, the internal and external elastic lamina are highly fenestrated. Finally, arterioles, the smallest of the true arteries, have only subendothelial elastic fibers (Fig. 1).

Elastic tissues in blood vessels endow connective tissue with resilience, permitting long-range deformability, as well as passive recoil without energy input. An appropriate ratio of elastin gives blood vessels suitable elasticity for their functions. During systole, elastic arteries expand and store potential energy, which during diastole is converted to the kinetic energy of blood flow because of the high ratio of elastin. In addition, these elastic components show a variety of structures based on hemodynamic characteristics such as blood pressure and vascular diameter (Wolinsky & Glagov, 1967; Carta et al., 2009; Wagenseil & Mecham, 2009; Basu et al., 2010). Conversely, hemodynamic characteristics are affected by elastic components. For example, elastin haploinsufficiency causes hypertension (Faury et al., 2003; Shifren et al., 2008). These hemodynamic functions of elastic fibers are known. However, elastin may control the cytoskeletal organization and proliferative activity of SMCs (Anidjar

Received September 28, 2012; accepted November 28, 2012
*Corresponding author. E-mail: aiji@okayama-u.ac.jp

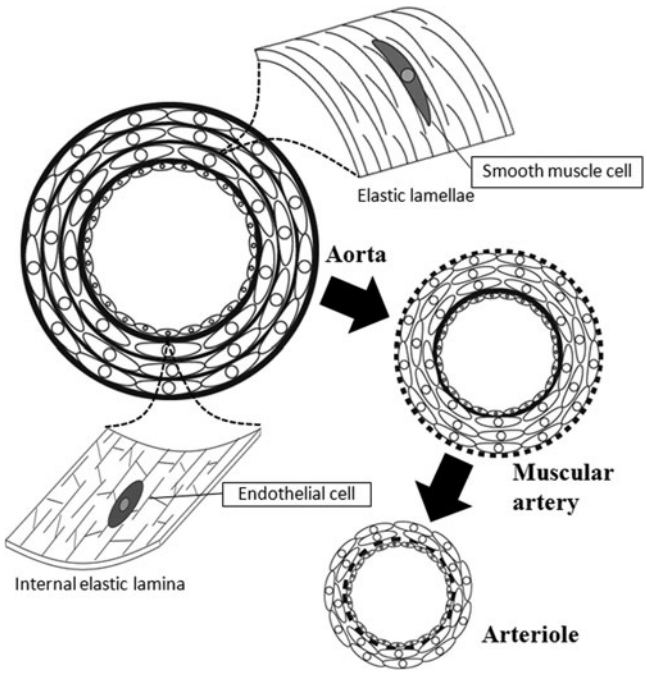

Figure 1. Structure of elastic fibers in arteries. Elastic fibers of the internal elastic lamina are arranged in parallel to the blood flow. Those of the elastic lamellae in the tunica media are arranged perpendicular to the blood flow. The aorta has internal elastic lamina and many elastic lamellae. The number of elastic lamellae in the tunica media decreases gradually as vessels come to the periphery. Therefore, muscular arteries have fewer elastic lamellae in the tunica media than in the aorta. The internal elastic lamina in arterioles is highly fenestrated.

et al., 1990; Kielty, 2006). Elastin is not simply a physical scaffold for the tissue, but it is also a physiologically significant scaffold in cells and is crucial for the maintenance of a tubular structure. In fact, a loss of function in one allele of the elastin gene causes the proliferation of SMCs, leading to supravalvular aortic stenosis (Brooke et al., 2003*a*). These elastic functions are maintained throughout the lifetime. However, various matrix degrading enzymes such as matrix metalloproteinases and serine proteases can cleave elastic fiber molecules (Karnik et al., 2003). Indeed, the loss of elasticity due to degradative changes is a major contributing factor in the aging of connective tissues and in the pathogenesis of arteriosclerosis and aortic aneurysms (Curran et al., 1993; Mochizuki et al., 2002; Brooke et al., 2003*b*).

There are many studies on the architecture of elastic fibers in the large arteries (Ushiki & Murakumo, 1991; Farand et al., 2007). Those studies used elastin's chemical resistance to strong acid in order to isolate elastin for biochemical analysis (Rasmussen et al., 1975; Daamen et al., 2005; Mecham, 2008). Although these procedures are useful for observing elastin-rich tissues such as those of the aorta, they are not suitable for small vessels such as arterioles because they easily collapse during specimen preparation. We have developed a new scanning electron microscopy (SEM) technique in which a vascular corrosion cast is used as a scaffold for small vessels prior to formic acid digestion. This study will demonstrate the applicability of the new method for evaluating the three-dimensional (3D) structures of arterioles and venules, and the association of their structures with hemodynamic state.

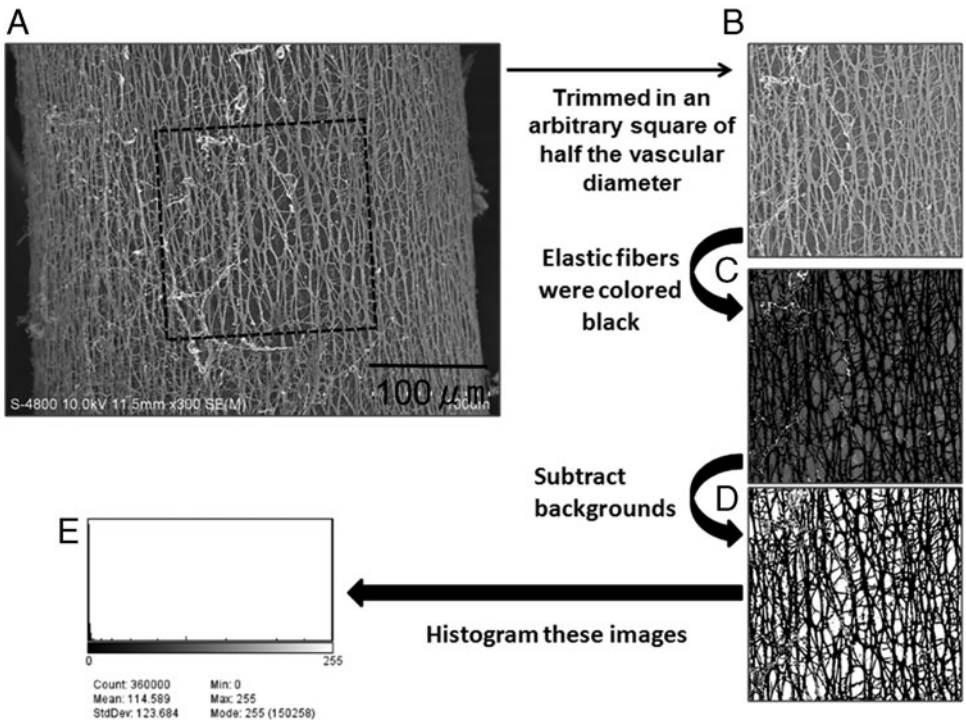

Figure 2. SEM image processing and analysis. **A**, **B:** SEM images were trimmed in an arbitrary square of half the length of the diameter in a well-focused area. **C:** Mesh fibers were colored black. **D:** Image with backgrounds subtracted. **E:** Image digitized for histograms.

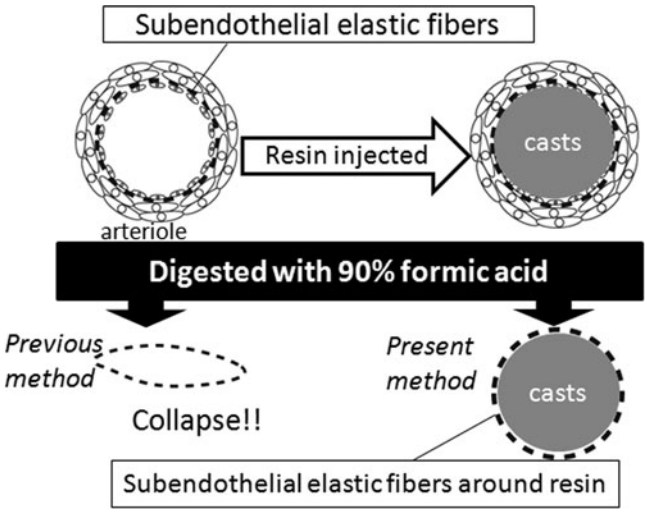

Figure 3. Present resin injection-digestion method. The previous method could not be used to digest arterioles because arterioles are too physically fragile. The present study successfully showed the 3D structures of elastic fibers in small vessels by utilizing the vascular cast as a scaffold.

Materials and Methods

Animals

The study used 6-week-old male Wistar rats: 10 rats for SEM, 2 for transmission electron microscopy (TEM), and 8 for amino acid analysis. The animals were deeply anesthetized with an overdose of ether inhalation, and a cannula was inserted into the thoracic aorta for successive perfusion. All procedures in this study conformed to the Guide for the Care and Use of Laboratory Animals, published by the U.S. National Institutes of Health, were approved by the Department of Animal Resources of the Advanced Science Research Center at Okayama University and were carried out in accordance with the Guidelines for Animal Experiments at Okayama University (OKU-201140). SEM of formic acid-digested components revealed three-dimensionally the elastic fiber architecture of arterioles and venules on the 3D level. Images obtained with TEM confirmed these findings two-dimensionally.

Tissue Preparation for Scanning Electron Microscopy

The cannulated thoracic aorta was flushed with Ringer's solution. It was then perfused with fixative solution containing 4% paraformaldehyde in 0.1 M phosphate buffer (pH 7.4) for 5 min, and then successively with Mercox resin (DIC Corporation, Tokyo, Japan). The resin polymerized for 10 min, after which the muscles of the abdominal wall were excised *en bloc* with their supplying blood vessels, and stored in 0.1 M phosphate buffer (pH 7.4).

The inferior epigastric artery and vein with their branches were pretreated with 10% formic acid at 45°C, dissected out, transferred into 90% formic acid at 45°C for 24 h, and finally rinsed in McIlvaine's citrate/phosphate buffer (pH 3.0) at room temperature for 12 h. These tissues were then treated with tannin-osmium methods (Murakami, 1973). The specimens were dehydrated through a graded series of ethanol and then freeze-dried with t-butanol in a freeze dryer (Hitachi ES-2030). Dried specimens were mounted onto aluminum stubs and coated with osmium (osmium plasma ion coater, HPC-1S, Vacuum Device Inc., Mito, Japan), and examined by SEM (Hitachi, S-4800, Central Research Laboratory, Okayama University Medical School).

Tissue Preparation for Transmission Electron Microscopy

The cannulated thoracic aorta was flushed with Ringer's solution and perfused with fixative solution containing 4% paraformaldehyde in 0.1 M phosphate buffer (pH 7.4) for 5 min. The dissected tissue segments were fixed in 2% glutaraldehyde in 0.1 M phosphate buffer (pH 7.4) for 2 to 4 days. The fixed tissues were washed twice with 0.1 M phosphate buffer (pH 7.4), transferred to 1% osmium tetroxide for 1 h, and then washed twice in distilled water. These specimens were then processed through a graded series of ethanol and embedded in epoxy resin (Epok 812, Okenshoji Co., Ltd, Tokyo, Japan). Ultrathin sections were cut and stained with 0.5% tannic acid, and were metal-stained with uranyl acetate and lead citrate. These specimens were then examined using a transmission electron microscope (Hitachi, H-7650, Central Research Laboratory, Okayama University Medical School).

SEM Image Processing and Analysis

To analyze mesh density, scanning micrographs were taken from five or three different segments to one artery or vein, respectively. In total, 50 images of arteries and 30 images of veins were collected and analyzed. SEM images of vessels were trimmed in an arbitrary square of half the vascular diameter at a well-focused central area (Figs. 2A, 2B). Mesh fibers were colored black as a different layer using a color picker tool and a manual painting tool in RGB color mode of Photoshop CS3 (Adobe Systems, San Jose, CA, USA) (Figs. 2B, 2C). In this process, mesh fibers were easily distinguished from casts and other debris in visual observation of SEM images. Image data were examined in random order by paired observers. After subtracting the original image layer (Figs. 2C, 2D), black (mesh fibers) and white (vascular casts and other debris) images were obtained. Such digitally processed images were used to analyze the density of mesh fibers. Black mesh fibers were separated by a filter of 0–128/256 using Image J version 1.41o (National Institutes of Health, Bethesda, MD, USA) (Fig. 2E). Their ratio of occupied to total area was then calculated as mesh fibers density.

Amino Acid Analysis

Fibers surrounding vascular casts after formic acid digestion were carefully collected to obtain two samples. One was collected from two rats, and the other from six. Samples were prepared as previously described (Shiratsuchi et al., 2010). Acid-digested specimens were hydrolyzed under vacuum with 6 M HCl for 48 h at 110°C, dried, and dissolved

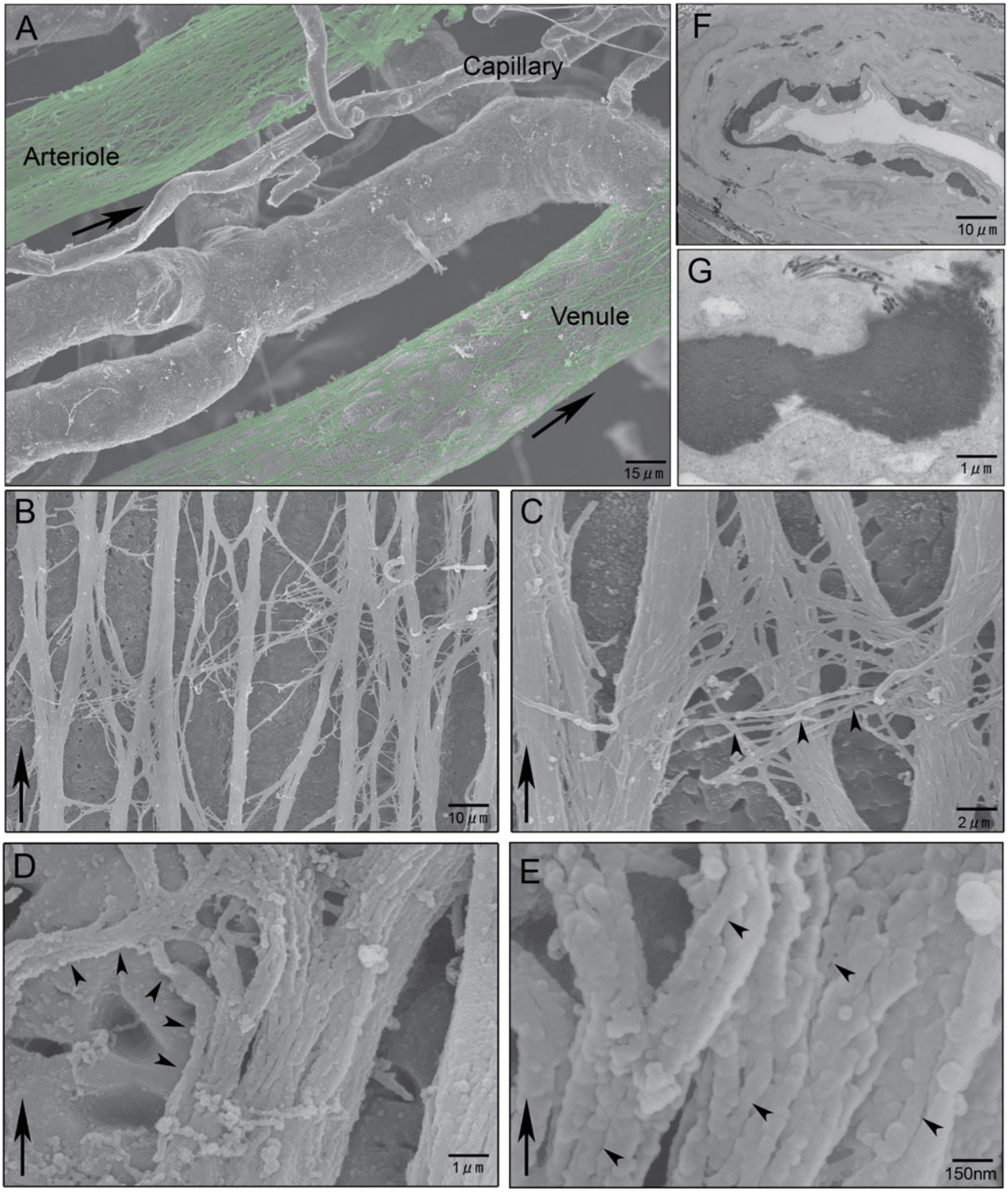

Figure 4. Details of subendothelial elastic architecture in blood vessels. **A:** Subendothelial elastic structure (green) of blood vessels looked like a mesh architecture by SEM following digestion treatment, in which vascular corrosion casts were used as a scaffold for small vessels. **B:** The long axis was parallel to the longitudinal direction of the vessels, and longitudinal mesh fibers were thicker. **C:** Some mesh fibers made skewed lines (arrowheads). **D:** Some of the mesh fibers made hairpin loops (arrowheads) at bifurcations of the meshwork. **E:** These mesh fibers were bundle of 50–100 nm diameter filaments (arrowheads). **F:** The subendothelial elastic architecture of the vessels was observed by TEM in tannic acid-stained samples. **G:** The 50–100 nm filaments composing mesh fibers were not observed in a high power view of TEM. **A–E:** The longitudinal direction of the vessels is indicated by arrows.

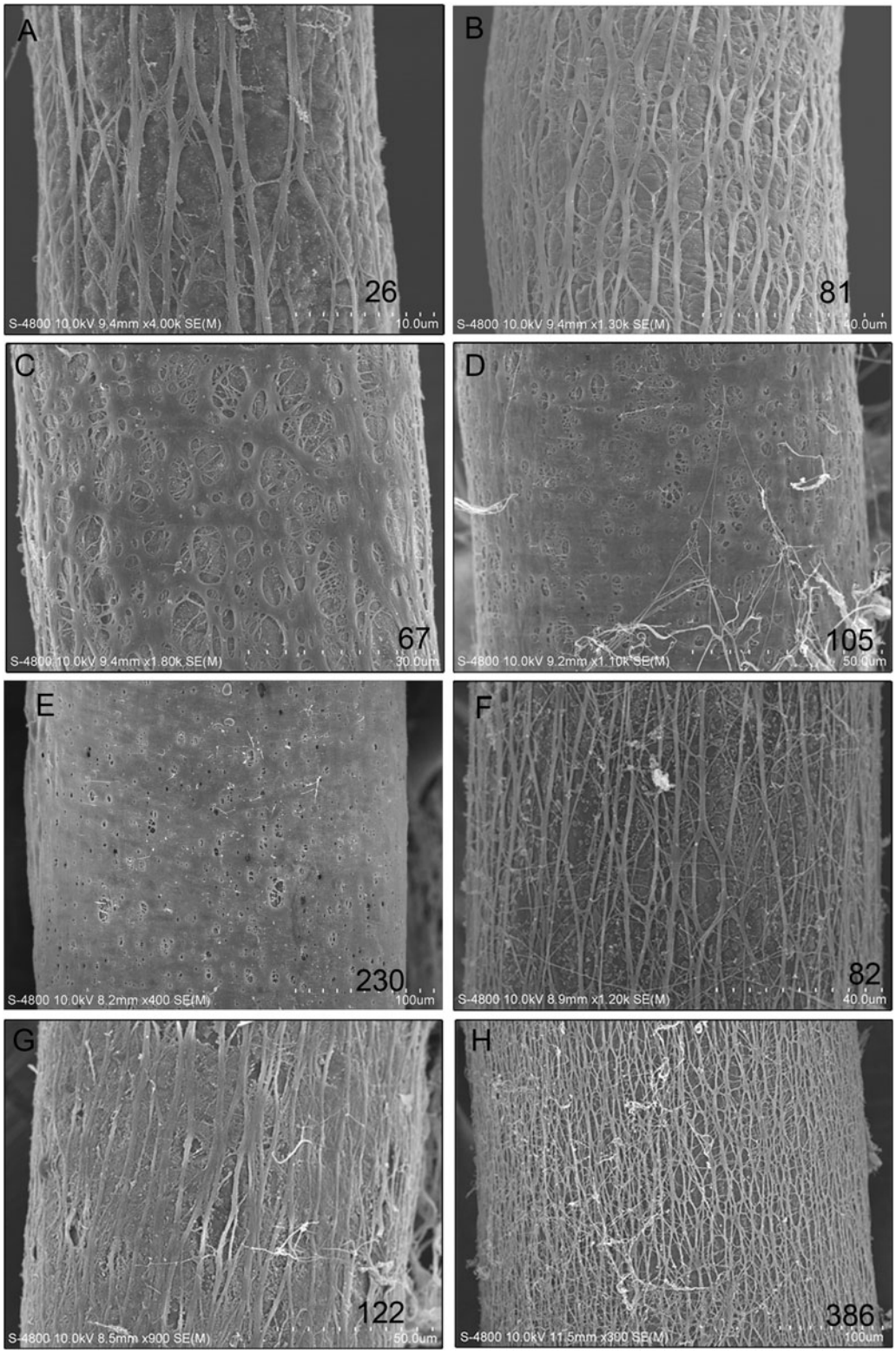

Figure 5. Subendothelial elastic architectures of various sizes of blood vessels. Vascular diameters are given in the lower right parts of the figures. **A:** An arteriole with a diameter of 18 μm found just before a capillary. A mesh architecture was observed. **B:** An arteriole with a diameter of 81 μm. The mesh architecture was the same as in panel **A**. **C:** An arteriole with a diameter of 67 μm. This had a honeycomb architecture. **D:** An arteriole with a diameter of 105 μm. The holes in the honeycomb became smaller. **E:** A small artery with a diameter of 230 μm. There were few holes and they were very small. Meshwork looked like a sheet. **F:** A venule with a diameter of 97 μm. **G:** A venule with a diameter of 122 μm. **H:** A venule with a diameter of 386 μm. The mesh architecture of the venules closely resembled that of the arterioles, but large venules maintained a mesh architecture.

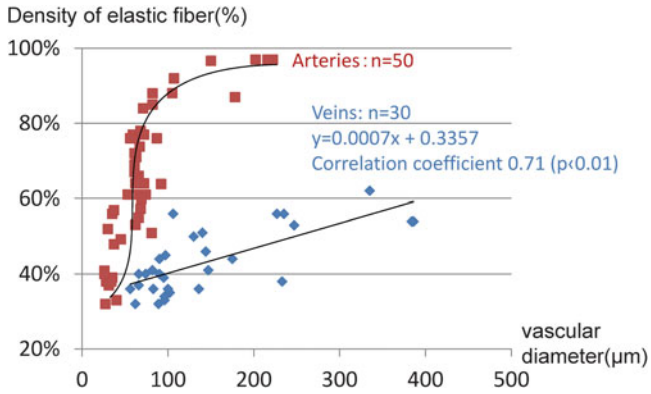

Figure 6. The relationships between mesh densities of elastic fibers and vascular diameters. The vertical axis is the density of elastic fibers, and the horizontal axis is the vascular diameter. Arteries and veins are marked with red squares and blue diamonds, respectively. The density-diameter relationships are represented by sigmoid curve in arteries, while these of veins are by linear fashion.

in 0.02 M HCl. Amino acid analysis was carried out on a JLC-500/V amino acid analyzer (JEOL Ltd., Tokyo, Japan), using lithium buffers with increasing pH.

Results

By virtue of its strong intermolecular cross-linking, elastin resisted strong formic acid treatment. SEM after this treatment visualized the 3D architecture of elastin as undigested components. By combining SEM with vascular casting as a scaffold, the current study successfully demonstrated the 3D architecture of elastic fibers in blood vessels of various sizes, even small vessels such as arterioles and venules (Fig. 3). The subendothelial elastic architecture of vessels looked like a meshwork regardless of the vascular types (Fig. 4A). The long axis of the meshwork was parallel to the longitudinal direction of the vessels, and the longitudinal mesh fibers were thicker than the traverse ones (Fig. 4B). These mesh fibers were on a single layer of meshwork, but sometimes they made skew lines to be on two or more layers of meshwork (Fig. 4C). These meshworks appeared in honeycomb patterns, in which large and small mesh holes formed by mesh fibers made hairpin loops or U-shapes (Fig. 4D). These mesh fibers were a bundle of 50–100 nm diameter filaments (Fig. 4E). TEM images confirmed thick fibers under the ECs. The mesh fibers had regular arrangements and the same diameters as observed by SEM. However, the TEM images of mesh fibers were homogeneous and showed neither 50–100 nm diameter filaments composing mesh fibers nor thin traversing mesh fibers linking the thick mesh fibers (Figs. 4F, 4G). As a result, the current methods using SEM reveal differences in vascular type and size, as well as the detailed course of elastic fibers.

Previous studies have indicated that the development of elastic components in large arteries is associated with hemodynamic characteristics, such as blood pressure and vascular diameter (Wolinsky & Glagov, 1967; Carta et al., 2009; Wagenseil & Mecham, 2009; Basu et al., 2010). However, the present SEM images show the relationship between the development of elastic components and vascular size in small blood vessels (Figs. 5, 6). Their relationship in veins exhibited a gradual linear increment with the density ranging from 30% to 60%. In contrast, their relationship in arteries is represented by an S-shaped curve with a steep increase from 50% to 80% at 75 μm (Fig. 6). These results indicated that elastic components developed with their vascular size, but differences in graph lines between arteries and veins may have resulted from another hidden developing factor, possibly blood pressure.

Various states of subendothelial elastic meshwork were observed. The density of the mesh architectures of crotch region was higher than that of neighbor regions (Figs. 7A, 7B). In the case of branching of small vessels from thick ones, regardless of the mesh density of parent vessel, the meshwork of the branched thin vessel showed proper mesh density as indicated in Figure 6 (Figs. 7C, 7D). SMCs saved from chemical digestion were crossed with subendothelial elastic fibers (Fig. 7E). One traversing fiber sometimes crossed over many longitudinal fibers (Fig. 7F).

The amino acid composition of elastin peptides obtained by formic acid digestive treatment is summarized in Table 1, which presents a set of data for one sample from six rats as an example. The acid treated samples showed an amino acid composition that was similar to the previously isolated bovine or porcine elastin, with abundant hydropho-

Table 1. Amino Acid Compositions of Elastin with Our Digestion Treatment.*

Amino Acid	Elastin with Digestion Treatment	Insoluble Elastin from Bovine[a]	Insoluble Elastin from Porcine[a]
Asp	8.81	6	6
Thr	17.78	9	14
Ser	16.61	9	11
Glu	22.14	16	19
Gly	346.91	330	330
Ala	213.63	228	234
Val	110.59	132	120
Met	0.34	0	0
Ile	23.63	24	18
Leu	59.96	60	54
Tyr	21.09	6	16
Phe	24.86	30	33
His	1.35	1	1
Lys	4.73	3	6
Ide+	0.88		
Des	1.32	15	3
Arg	9.51	6	6
Hyp	11.97	8	11
Pro	103.04	116	117

*Values are expressed per 1,000 amino acid residues.
[a]Data cited from Shiratsuchi et al. (2010).

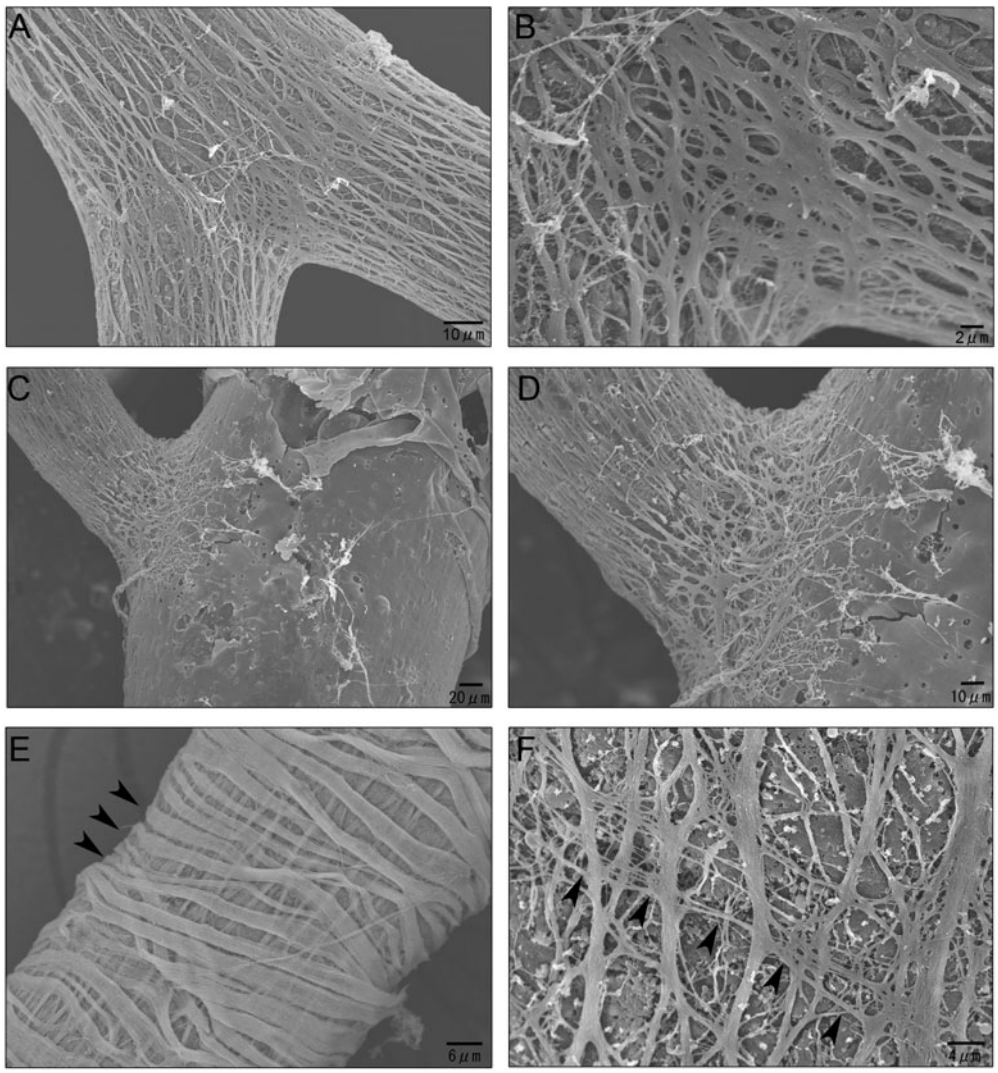

Figure 7. Various states of subendothelial elastic fibers architecture. **A:** The mesh density of the crotch region was higher than that of neighbor regions. **B:** This is a high power field of panel **A**. **C:** In the case of the branching of small vessels from thick ones, regardless of the mesh density of the parent vessel, the meshwork of the branched thin vessel showed a proper mesh density as indicated in Figure 6. **D:** This is a high power field of panel **C**. **E:** This specimen was not fully digested, and SMCs (arrowheads) of tunica media surround and cross the mesh fibers. **F:** One traversing mesh fiber (arrowhead) crosses over many longitudinal mesh fibers.

bic residues such as alanine and valine and with trace amounts of methionine (Shiratsuchi et al., 2010).

Discussion

An SEM analysis of the 3D architectures of elastic fibers has been limited to large arteries because small vessels such as arterioles are too physically fragile for the isolation procedure (Ushiki & Murakumo, 1991; Ushiki, 1992; Sato et al., 1994; Farand et al., 2007). The present study displayed the 3D architectures of elastic fibers in small vessels by utilizing the vascular cast as a scaffold. And the elastin components reproduced in the current formic acid digested specimens were identified as pure elastin by amino acid analysis; such biochemical analysis of digested specimens had not been done previously.

Previous studies showed that ECs cooperate with each other to make honeycomb arrangements of microfibrils around them with a core of elastic fibers (Weber et al., 2002; Kielty, 2006), and the arrangement of elastic fibers reflects the long axes of these cells. The present study showed that the subendothelial elastic fibers assemble into a meshwork sheet, whose long axis runs parallel to the longitudinal direction of the vessels and is perpendicular to the SMCs. The subendothelial elastin fibers were located between the endothelium and the smooth muscle of the tunica media. The ECs were arranged longitudinally, while the muscular cells were arranged circularly. We speculated that the longitudinally oriented meshwork fibers may be produced by longitudinal cells, probably ECs, and that mesh outer fibers running across inner fibers (Figs. 3C, 7F) might be involved with other elements such as SMCs.

Previous studies had indicated that, in the aorta, the number of elastic lamella was related linearly to tensional forces within the wall (Wolinsky & Glagov, 1967; Wagenseil & Mecham, 2009). The present study demonstrated the relationship between the elastic component and vascular diameter of small blood vessels. These phenomena can be explained by Laplace's law that vascular wall tension (T) is represented by the multiplication of the intraluminal pressure (P) by the vascular radius (r); T (dyn/μm) = P (dyn/μm^2) r (μm) (Fowler, 1971). Larger arteries and veins have higher mesh densities than smaller ones because T is defined by r; an artery needs a high-density mesh architecture because it has high intraluminal pressure, whereas veins need a low-density mesh and a narrow range of density changes because they are exposed to few changes in intraluminal pressure. A sudden change in the mesh density in arterioles from 100 μm to 50 μm might indicate a turning point in intraluminal pressure. The mesh architecture at a bifurcation site reflects Laplace's law. Branching blood vessels with the same diameter have the same mesh density (Fig. 7A). However, their mesh density is obviously different if they have a different radius (Fig. 7C). Shear stress, in addition to intraluminal pressure, may affect mesh density because crotches at a bifurcation site have a higher density mesh than the surrounding walls (Fig. 7B). Therefore, blood vessels have a suitable skeleton for their hemodynamic state.

Many pathophysiological models have shown changes in elastic fibers (Seyama et al., 1990; Wagenseil et al., 2007, 2010; Muiznieks et al., 2010; Wachi, 2011). Moreover, in the genes controlling elastic fiber deposition, there are a lot of mutations that might cause structural changes in the fibers and might also participate in the development of cardiovascular diseases in general and hypertension in particular. For example, supravalvular aortic stenosis (SVAS) is caused by a large spectrum of mutations including point mutations, translocations, and partial deletions within the elastin gene. SVAS is associated with the proliferation of SMCs, the obstruction of arteries, thinner elastic lamellae, and an increased number of lamellar units causing hypertension in clinical condition (Dridi et al., 2005). Marfan syndrome is caused by mutations in the gene coding for microfibrillar proteins, fibrillin-1 and fibrillin-2. Marfan syndrome is associated with the rupture of elastic fibers and the necrosis of SMCs in the tunica media, causing aortic dissection, pulse pressure elevation, and aneurisms (Jondeau et al., 2011). The fact that mutations of elastic fibers have been linked to abnormal vascular structure and, in some cases, the development of hypertension raises the possibility that polymorphisms of these genes may occur in association with human essential hypertension. However, the structural changes of elastic fibers until now could not be clearly observed in detail because there was no technique to observe the delicate elastic fiber architecture of small vessels. The use of the current methods is therefore expected to reveal the structural changes in elastic fiber in pathologic models.

Conclusion

This new method was found to be useful for investigating the subendothelial elastic fibers of small vessels. The results showed that these fibers form honeycomb patterns that contain longitudinal fibers and 3D meshworks. In addition, their development may be associated with hemodynamic characteristics.

Acknowledgments

We thank M. Narasaki for his valuable TEM technical assistance. This work was supported by a Grant-in-Aid for Scientific Research from JSPS (22591542 to A.O.)

References

Anidjar, S., Salzmann, J.L., Gentric, D., Lagneau, P., Camilleri, J.P. & Michel, J.B. (1990). Elastase-induced experimental aneurysms in rats. *Circulation* **82**, 973–981.

Basu, P., Sen, U., Tyagi, N. & Tyagi, S.C. (2010). Blood flow interplays with elastin: collagen and MMP: TIMP ratios to maintain healthy vascular structure and function. *Vasc Health Risk Manag* **6**, 215–228.

Brooke, B.S., Bayes-Genis, A. & Li, D.Y. (2003*a*). New insights into elastin and vascular disease. *Trends Cardiovasc Med* **13**, 176–181.

Brooke, B.S., Karnik, S.K. & Li, D.Y. (2003*b*). Extracellular matrix in vascular morphogenesis and disease: Structure versus signal. *Trends Cell Biol* **13**, 51–56.

Carta, L., Wagenseil, J.E., Knutsen, R.H., Mariko, B., Faury, G., Davis, E.C., Starcher, B., Mecham, R.P. & Ramirez, F. (2009). Discrete contributions of elastic fiber components to arterial development and mechanical compliance. *Arterioscler Thromb Vasc Biol* **29**, 2083–2089.

Curran, M.E., Atkinson, D.L., Ewart, A.K., Morris, C.A., Leppert, M.F. & Keating, M.T. (1993). The elastin gene is disrupted by a translocation associated with supravalvular aortic stenosis. *Cell* **73**, 159–168.

Daamen, W.F., Hafmans, T., Veerkamp, J.H. & van Kuppevelt, T.H. (2005). Isolation of intact elastin fibers devoid of microfibrils. *Tissue Eng* **11**, 1168–1176.

Dridi, S.M., Foucault, B.A., Igondjo, T.S., Senni, K., Ejeil, A.L., Pellat, B., Lyonnet, S., Bonnet, D., Charpiot, P. & Godeau, G. (2005). Vascular wall remodeling in patients with supravalvular aortic stenosis and Williams Beuren syndrome. *J Vasc Res* **42**, 190–201.

Farand, P., Garon, A. & Plante, G.E. (2007). Structure of large arteries: Orientation of elastin in rabbit aortic internal elastic lamina and in the elastic lamellae of aortic media. *Microvasc Res* **73**, 95–99.

Faury, G., Pezet, M., Knutsen, R.H., Boyle, W.A., Heximer, S.P., McLean, S.E., Minkes, R.K., Blumer, K.J., Kovacs, A., Kelly, D.P., Li, D.Y., Starcher, B. & Mecham, R.P. (2003). Developmental adaptation of the mouse cardiovascular system to elastin haploinsufficiency. *J Clin Invest* **112**, 1419–1428.

Fowler, N.O. (1971). Law of Laplace. *N Engl J Med* **285**, 1087–1088.

Hirai, M., Ohbayashi, T., Horiguchi, M., Okawa, K., Hagiwara, A., Chien, K.R., Kita, T. & Nakamura, T. (2007). Fibulin-5/DANCE has an elastogenic organizer activity that is abrogated by proteolytic cleavage *in vivo*. *J Cell Biol* **26**, 1061–1071.

Jondeau, G., Michel, J.B. & Boileau, C. (2011). The translational science of Marfan syndrome. *Heart* **97**, 1206–1214.

Karnik, S.K., Brooke, B.S., Bayes-Genis, A., Sorensen, L., Wythe, J.D., Schwartz, R.S., Keating, M.T. & Li, D.Y. (2003). A critical role for elastin signaling in vascular morphogenesis and disease. *Development* **130**, 411–423.

Kielty, C.M. (2006). Elastic fibres in health and disease. *Expert Rev Mol Med* **8**, 1–23.

Kielty, C.M., Sherratt, M.J. & Shuttleworth, C.A. (2002). Elastic fibres. *J Cell Sci* **115**, 2817–2828.

Mecham, R.P. (2008). Methods in elastic tissue biology: Elastin isolation and purification. *Methods* **45**, 32–41.

Mochizuki, S., Brassart, B. & Hinek, A. (2002). Signaling pathways transduced through the elastin receptor facilitate proliferation of arterial smooth muscle cells. *J Biol Chem* **277**, 44854–44863.

Muiznieks, L.D., Weiss, A.S. & Keeley, F.W. (2010). Structural disorder and dynamics of elastin. *Biochem Cell Biol* **88**, 239–250.

Murakami, T. (1973). A metal impregnation method of biological specimens for scanning electron microscopy. *Arch Histol Jap* **35**, 323–326.

Rasmussen, B.L., Bruenger, E. & Sandberg, L.B. (1975). A new method for purification of mature elastin. *Anal Biochem* **64**, 255–259.

Sato, F., Shimada, T., Kitamura, H., Campbell, G.R. & Ogata, J. (1994). Changes in morphology of elastin fibers during development of the tunica intima of monkey aorta. *Heart Vessels* **9**, 140–147.

Seyama, Y., Hayashi, M., Usami, E., Tsuchida, H., Tokudome, S. & Yamashita, S. (1990). Basic study on non-delipidemic fractionation of aortic connective tissue of human and experimental atherosclerosis. *Jpn J Cli Chem* **19**, 87–93.

Shifren, A., Durmowicz, A.G., Knutsen, R.H., Faury, G. & Mecham, R.P. (2008). Elastin insufficiency predisposes to elevated pulmonary circulatory pressures through changes in elastic artery structure. *J Appl Physiol* **105**, 1610–1619.

Shiratsuchi, E., Ura, M., Nakaba, M., Maeda, I. & Okamoto, K. (2010). Elastin peptides prepared from piscine and mammalian elastic tissues inhibit collagen-induced platelet aggregation and stimulate migration and proliferation of human skin fibroblasts. *J Pept Sci* **16**, 652–658.

Ushiki, T. (1992). Preserving the original architecture of elastin components in the formic acid-digested aorta by an alternative procedure for scanning electron microscopy. *J Electron Microsc (Tokyo)* **41**, 60–63.

Ushiki, T. & Murakumo, M. (1991). Scanning electron microscopic studies of tissue elastin components exposed by a KOH-collagenase or simple KOH digestion method. *Arch Histol Cytol* **54**, 427–436.

Wachi, H. (2011). Role of elastic fibers on cardiovascular disease. *J Health Sci* **57**, 449–457.

Wagenseil, J.E., Ciliberto, C.H., Knutsen, R.H., Levy, M.A., Kovacs, A. & Mecham, R.P. (2010). The importance of elastin to aortic development in mice. *Am J Physiol Heart Circ Physiol* **299**, 257–264.

Wagenseil, J.E., Knutsen, R.H., Li, D.Y. & Mecham, R.P. (2007). Elastin-insufficient mice show normal cardiovascular remodeling in 2K1C hypertension despite higher baseline pressure and unique cardiovascular architecture. *Am J Physiol Heart Circ Physiol* **293**, 574–582.

Wagenseil, J.E. & Mecham, R.P. (2009). Vascular extracellular matrix and arterial mechanics. *Physiol Rev* **89**, 957–989.

Weber, E., Rossi, A., Solito, R., Sacchi, G., Agliano, M. & Gerli, R. (2002). Focal adhesion molecules expression and fibrillin deposition by lymphatic and blood vessel endothelial cells in culture. *Microvasc Res* **64**, 47–55.

Wise, S.G. & Weiss, A.S. (2009). Tropoelastin. *Int J Biochem Cell Biol* **41**, 494–497.

Wolinsky, H. & Glagov, S. (1967). A lamellar unit of aortic medial structure and function in mammals. *Circ Res* **20**, 99–111.